Effect of hybridization symmetry on topological phases of odd-parity multiband superconductors

T.O. Puel[1],* P.D. Sacramento[1,2], and M. A. Continentino[1]
[1] *Centro Brasileiro de Pesquisas Físicas, Rua Dr. Xavier Sigaud, 150, Urca 22290-180, Rio de Janeiro, RJ, Brazil and*
[2] *CeFEMA, Instituto Superior Técnico, Universidade de Lisboa, Av. Rovisco Pais, 1049-001 Lisboa, Portugal*
(Dated: August 16, 2016)

We study two-band one-dimensional superconducting chains of spinless fermions with inter and intra-band pairing. These bands hybridize and, depending on the relative angular momentum of their orbitals, the hybridization can be symmetric or anti-symmetric. The self-consistent competition between intra and inter-band superconductivity and how it is affected by the symmetry of the hybridization is investigated. In the case of anti-symmetric hybridization the intra and inter-band pairings do not coexist while in the symmetric case they do coexist and the interband pairing is shown to be dominant. The topological properties of the model are obtained through the topological invariant winding number and the presence of edge states. We find the existence of a topological phase due to the inter-band superconductivity and induced by symmetric hybridization. In this case we find a characteristic 4π-periodic Josephson current. In the case of anti-symmetric hybridization we also find a 4π-periodic Josephson current in the gapless inter-band superconducting phase, recently identified to be of Weyl-type.

arXiv:1601.07609v2 [cond-mat.supr-con] 14 Aug 2016

I. INTRODUCTION

Multiband models for the superconducting state and their topological properties have received increasing attention recently [1–6]. This consideration has been important to explain many important effects in topological systems. For instance, topological semimetals [7] and chiral superfluidity [8] have been predicted in multiorbital models where orbitals with different symmetries interact. Two component fermionic systems with occupied s and p orbital states were shown to have a rich phase diagram in both one and two dimensions [4]. A general connection between multiband and multicomponent superconductivity has also been made [9]. Topological properties in three-band models were also studied [10–13].

It is well known that the Kitaev model [14–16] – antisymmetric pairs of spinless fermions in 1D – is the simplest model that exhibits a topological phase with Majorana modes in the ends of a p-wave chain, depending on the state of the system. The topological non-trivial phase presents Majorana fermions at its ends. Otherwise, the chain is in a superconducting phase with trivial topological properties and has no end states[16]. An extension of this effective spinless fermions model for a multiband hybridized system comprised of the Su, Schrieffer and Heeger (SSH) model[17] and the Kitaev model was done in Ref. [18], where topological properties are discussed showing edge states that are of Majorana and fermionic types.

Triplet superconductivity is rare in nature. Thus, the pursuit of alternatives to create triplet superconductivity lead to engineering a topological insulating chain (made with strong spin-orbit material) in proximity of a normal superconductor and in the presence of an applied magnetic field [19, 20]. On the other hand, triplet pairing has been found to be physically realizable in some systems. In Ref. [6] it was shown that odd-parity superconductivity occurs in superconducting (SC) multilayers, where this state is a symmetry-protected topological state. In addition, triplet pairing is found in ^{3}He [21] and in Sr_2RuO_4[22], as well as in some rare noncentrosymmetric systems [23]. Triplet pairing was also studied in the context of extended Hubbard chain [24].

Motivated by the recently discussed topological characters of multiband models[4, 6], and based on the simplest model that describes the topological properties of a chain of spinless fermions, we study the Kitaev model with two orbital-bands. We include and discuss inter- and intraband superconducting couplings. A characteristic feature of multiband systems is the hybridization between the different orbitals. This arises from the superposition of the wave functions of these orbitals in different sites. It can have distinct symmetry properties depending on the orbitals involved. If this mixing involves orbitals with angular momenta that differ by an odd number, hybridization turns out to be anti-symmetric, i.e., in real space we have $V_{ij} = -V_{ji}$ or in momentum, k-space, $V(-k) = -V(k)$. Otherwise hybridization is symmetric respecting inversion symmetry in different sites [25].

The bulk-edge correspondance guarantees that in the topological phases there are subgap edge states. In the case of a topological superconductor, zero energy Majorana modes are predicted to appear and great effort has been devoted to prove their existence. Methods that provide signatures of their presence have been proposed and experimentally tested via for instance tunneling experiments [26, 27], interferometry [16], point contacts using the Andreev reflection [28] through the detection of zero-bias peaks [29], using the quantum waveguide theory [30] which gives the correct bulk-edge correspondence [31] and fractional Josephson currents [14, 16, 32]. Also

* tharnier@me.com

signatures of the Majorana states may be found in bulk measurements such as the imaginary part of frequency dependent Hall conductance [33] and the d.c. Hall conductivity itself [34].

The existence of topological phases is detected in this work numerically calculating the winding number and by showing the existence of edge states at the ends of the chain. In addition, we calculate the Josephson current accross the junction between two superconductors to identify regimes where the periodicity of the Josephson current on the phase differences between the superconductors (original proposal by Kitaev[14]) or the equivalent situation of a superconducting ring threaded by a magnetic flux and interrupted by an insulator changes from the usual value of 2π to a 4π value [35]. As shown before [14, 35–45] the existence of the Majoranas at the edges allows tunneling of a single fermion at zero-bias leading to a $4\pi-$periodic current in contrast to the usual Cooper pair transport accross the junction which leads to the usual $2\pi-$periodic current. Experimental realization to detect 4π-periodic Josephson junction has been presented in Ref. [46] and an application to multiband systems has recently been presented in Ref. [47].

This paper is organized as follows. In section II we define the general Hamiltonian including symmetric and anti-symmetric hybridization. Also we proceed with the self-consistent calculations of the superconducting order parameters related to the competition between the intra- and inter-band pairings. The topological properties of the model are discussed in section III. We show a general calculation of the winding number when particle-hole symmetry is present in a 4×4 Bogoliubov-de Gennes (BdG) Hamiltonian. Also, we calculate the energy spectrum of a finite one-dimensional chain. The differences between trivial and topological phases are discussed from the perspective of zero-energy states. We also make the equivalence of the topological regimes with the 4π periodicity of the Josephson current. Finally, in section IV we present the conclusions and review the main results.

II. MODEL AND SELF-CONSISTENT CALCULATIONS

We consider a two-band superconductor with hybridization and triplet pairing in 1D, i.e., a chain of sites supporting two orbitals, let's say orbitals A and B. The pairing between fermions may exist on different bands (inter-band) or in each band (intra-band) and are always of p-wave type, in the sense that pairs of spinless fermions are spatially anti-symmetric. The problem can be viewed as a generalization of the Kitaev model to two orbitals. We also have the hybridization term between the orbitals A and B that may be symmetric or anti-symmetric. The simplest Hamiltonian in momentum space that describes those types of superconductivity and hybridization may be written as $\mathcal{H}=\mathcal{H}_0+\mathcal{H}_h+\mathcal{H}_{SC}$ where the kinetic part is

$$\mathcal{H}_0=\sum_k\left\{\left(\varepsilon_k^A-\mu\right)a_k^\dagger a_k+\left(\varepsilon_k^B-\mu\right)b_k^\dagger b_k\right\},\quad(1)$$

where $a_k^\dagger\left(b_k^\dagger\right)$ is the creation operator of spinless fermion at $A\,(B)$-band with momentum k. Also, μ is the chemical potential and we choose $\varepsilon_k^A=-\varepsilon_k^B=2t\cos(k)\equiv\varepsilon_k$ where t is the hopping amplitude. The hybridization term is

$$\mathcal{H}_h=\sum_k\left\{V(k)\,a_k^\dagger b_k-V(-k)\,b_{-k}a_{-k}^\dagger+\text{h.c.}\right\},\quad(2)$$

where $V(k)=2iV_{\text{as}}\sin(k)\equiv V_{\text{as},k}$ if the hybridization is anti-symmetric or $V(k)=2V_{\text{s}}\cos(k)\equiv V_{\text{s},k}$ if the hybridization is symmetric, and V is the hybridization amplitude. Finally, the mean-field superconducting contribution to the Hamiltonian is

$$\begin{aligned}\mathcal{H}_{SC}=\sum_k\Big\{&\Delta_k a_k^\dagger b_{-k}^\dagger+\Delta_k b_k^\dagger a_{-k}^\dagger\\&+\Delta_{A,k}a_k^\dagger a_{-k}^\dagger+\Delta_{B,k}b_k^\dagger b_{-k}^\dagger+\text{h.c.}\Big\},\end{aligned}\quad(3)$$

with $\Delta_k=i\Delta\sin(k)$ where Δ is the superconducting inter-band pairing amplitude, and $\Delta_{(\text{A,B}),k}=i\Delta_{(\text{A,B})}\sin(k)$ where Δ_{A} and Δ_{B} are the superconducting intra-band pairing amplitudes. We could also include a superconducting term that changes Cooper pairs between different orbitals, which in terms of two particles interaction may be written as $\sum_{k,k'}g_J(k,k')\left(b_k^\dagger b_{-k}^\dagger a_{-k'}a_{k'}+a_k^\dagger a_{-k}^\dagger b_{-k'}b_{k'}\right)$, where g_J is the interaction strength. Without fluctuation, i.e., in the BCS theory, this term appears as an additive parameter to Δ_{A} and Δ_{B}, thus besides enhancing the intra-band superconductivity it does not change qualitatively the topological properties of the Hamiltonian considered here.

In the more compact BdG form, the Hamiltonian may be written in the Nambu representation [48] as $\mathcal{H}=\sum_k\boldsymbol{C}_k^\dagger\mathcal{H}_k\boldsymbol{C}_k$, where $\boldsymbol{C}_k^\dagger=\left(a_k^\dagger b_k^\dagger a_{-k}b_{-k}\right)$ and

$$\begin{aligned}\mathcal{H}_k=&-\mu\Gamma_{z0}-\varepsilon_k\Gamma_{zz}+\Delta_k\Gamma_{yx}\\&+\Delta_{\text{A},k}\frac{1}{2}\left(\Gamma_{y0}+\Gamma_{yz}\right)+\Delta_{\text{B},k}\frac{1}{2}\left(\Gamma_{y0}-\Gamma_{yz}\right)\\&+V_k\cdot\mathbb{I},\end{aligned}\quad(4)$$

where $\Gamma_{ij}=\tau_i\otimes s_j,\quad\forall\ i,j=0,x,y,z$; τ and s are the Pauli matrices acting on particle-hole and sub-band spaces, respectively, and $s_0=\tau_0$ are the 2×2 identity matrices. With respect to the Hamiltonian parameters: $V_k=-V_{\text{as},k}\boldsymbol{\Gamma}_{zy}$ if the hybridization is anti-symmetric or $V_k=V_{\text{s},k}\boldsymbol{\Gamma}_{zx}$ if the hybridization is symmetric.

In this section we present self-consistent results for the superconducting parameters Δ, Δ_{A} and Δ_{B} using the BdG formalism. The Hamiltonian defined in Eq. (4) can be solved using BdG transformations as $a_k=\sum_n\left[u_{n,k}^a\gamma_{n,k}+\left(v_{n,k}^a\right)^*\gamma_{n,-k}^\dagger\right]$ and $b_k=$

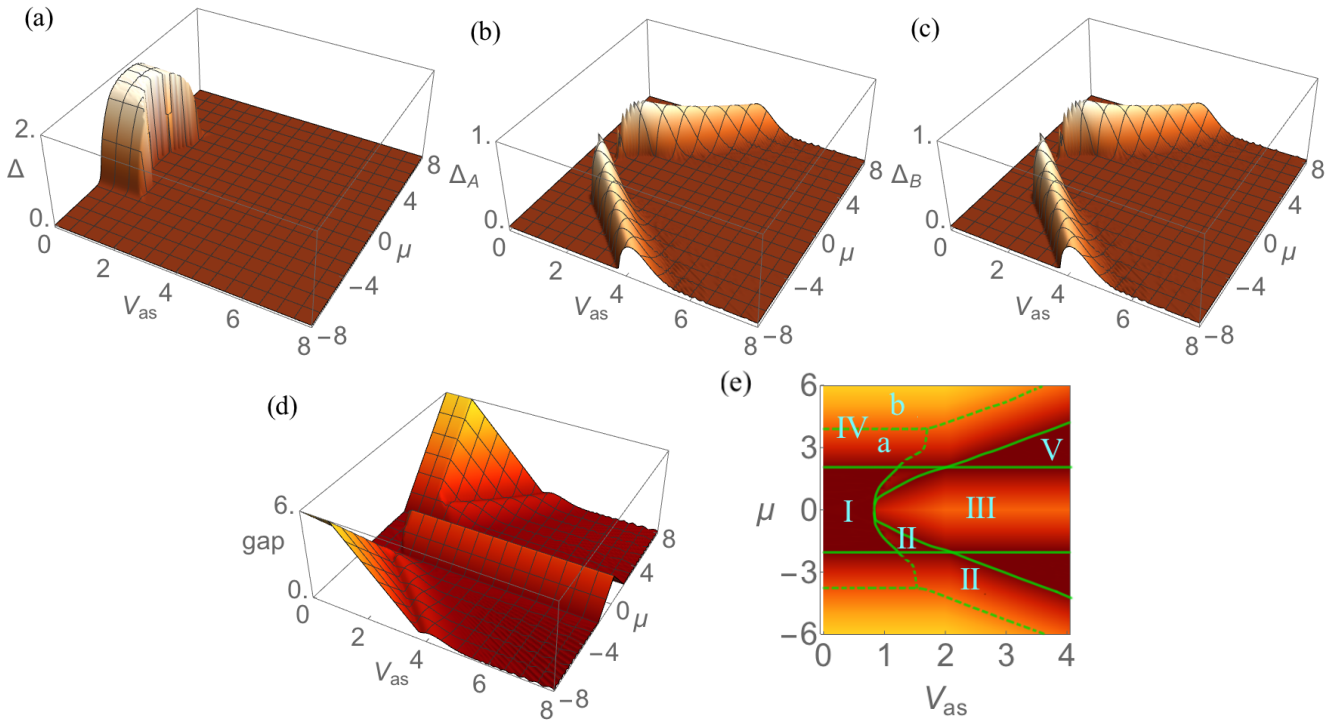

Figure 1. The first row shows the self-consistent solutions of the superconducting parameters, considering anti-symmetric hybridization. The order parameters calculated are the inter-band (Δ) and the intra-band ($\Delta_{A,B}$) ones. For instance, according to the anti-symmetric hybridization, A and B could be the orbitals s and p. For these results we set $g/2 = g_{\rm A} = g_{\rm B} = 1.7$. Second row shows the corresponding energy spectrum gap and the phase diagram. Phase I is a gapless inter-band superconducting phase. II is a gapped intra-band superconducting phase. III is a topological insulating phase. IVa shows a trivial gapped inter-band SC. IVb is a trivial insulating phase. Finally, V is a metallic phase. The phase diagram is symmetric around $\mu = 0$.

$\sum_n \left[u^b_{n,k}\gamma_{n,k} + \left(v^b_{n,k}\right)^* \gamma^\dagger_{n,-k}\right]$. This transformation diagonalizes the Hamiltonian in the form $\mathcal{H}_k\psi_n = E_n\psi_n$, with $\psi_n = \left(u^a_{n,k}\ \ u^b_{n,k}\ \ v^a_{n,-k}\ \ v^b_{n,-k}\right)^T_n$, where E_n are the energy eigenvalues and the wave function spinors ψ_n are the eigenstates.

The self-consistent solution implies that the pairings can be obtained using

$$\Delta = g\frac{1}{L}\sum_k i\sin(k)\left(\langle a_k b_{-k}\rangle + \langle b_k a_{-k}\rangle\right), \tag{5}$$

$$\Delta_{\rm A} = g_{\rm A}\frac{2}{L}\sum_k i\sin(k)\langle a_k a_{-k}\rangle, \tag{6}$$

$$\Delta_{\rm B} = g_{\rm B}\frac{2}{L}\sum_k i\sin(k)\langle b_k b_{-k}\rangle, \tag{7}$$

where g, $g_{\rm A}$ and $g_{\rm B}$ are the strength of the interactions between fermions in different orbitals, in orbitals A and in orbitals B, respectively. At zero temperature, using the representation of fermionic operators in terms of the Bogoliubov coefficients, we may write

$$\Delta = g\frac{1}{L}\sum_k\sum_n i\sin(k)\left[u^a_{n,k}\left(v^b_{n,-k}\right)^* + u^b_{n,k}\left(v^a_{n,-k}\right)^*\right], \tag{8}$$

$$\Delta_{\rm A} = g_{\rm A}\frac{2}{L}\sum_k\sum_n i\sin(k)\,u^a_{n,k}\left(v^a_{n,-k}\right)^*, \tag{9}$$

$$\Delta_{\rm B} = g_{\rm B}\frac{2}{L}\sum_k\sum_n i\sin(k)\,u^b_{n,k}\left(v^b_{n,-k}\right)^*. \tag{10}$$

A. Anti-symmetric hybridization

We first consider the case of anti-symmetric hybridization ($V_{\rm as}$) that occurs when the orbitals angular momenta have different parities, like orbitals s and p. In Fig 1 we show the results for the three order parameters calculated self-consistently, when $g/2 = g_{\rm A} = g_{\rm B} = 1.7$. A similar model was considered before [49] with only inter-band pairing. The strength of the coupling g only changes the superconducting amplitude of the SC phases (inter- or intra-band ones), thus its choice does not change qualitatively the results presented. It is interesting to point out that the self-consistent results for the superconduct-

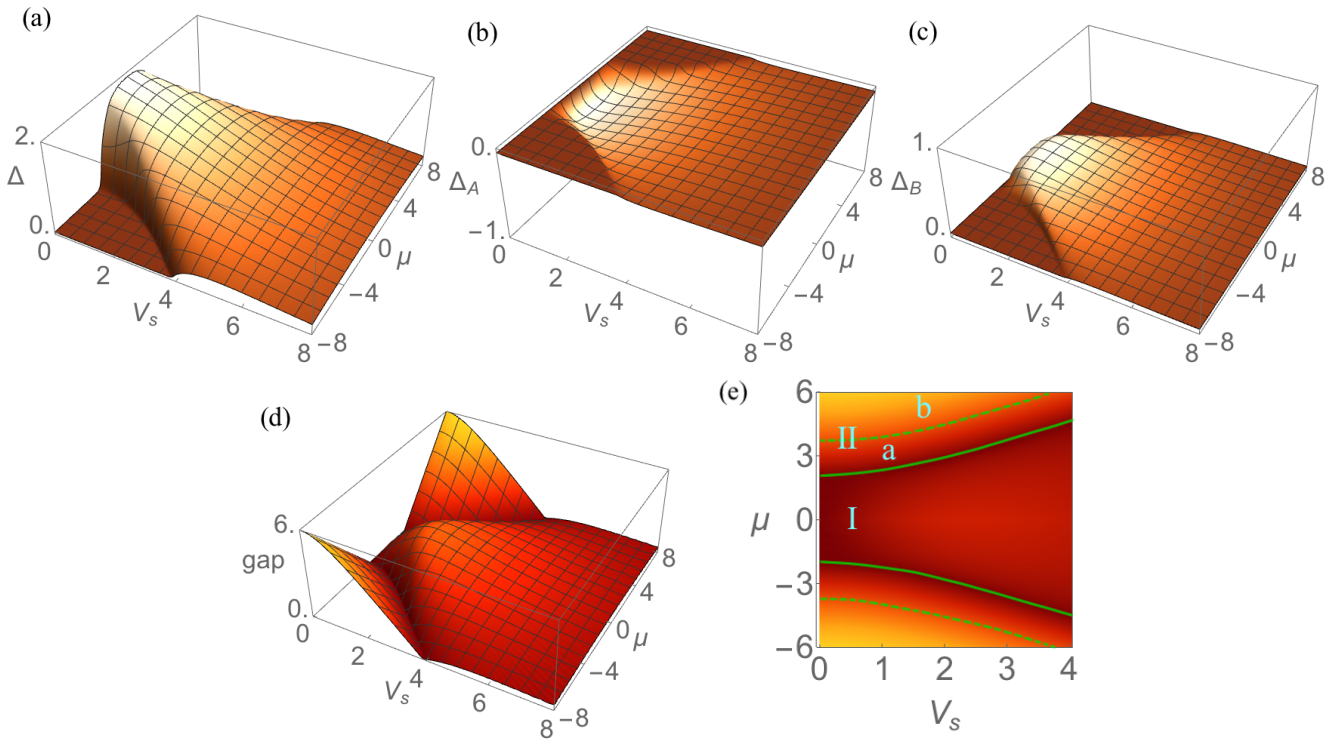

Figure 2. First row shows the self-consistent solutions of the superconducting parameters, considering symmetric hybridization. The order parameters calculated are the inter-band (Δ) and the intra-band ($\Delta_{A,B}$). For instance, according to the symmetric hybridization, A and B could be the orbitals s and d. For these results we set $g/2 = g_{\rm A} = g_{\rm B} = 1.7$. Second row shows the corresponding spectral gap and the phase diagram. Phase I carries both types of pairings and has non-trivial topological properties. Phase IIa is a gapped superconducting phase also with both inter- and intra-band pairings, but trivial topological properties. Phase IIb is a normal insulator. The phase diagram is symmetric around $\mu = 0$.

ing order parameters may converge to different results depending on the initial guesses. This is a consequence of the first order nature of the quantum phase transitions between the different ground states. Therefore it is necessary to calculate the energy of the different states to obtain the true ground state for a given set of parameters.

We note first that inter and intra-band superconductivity do not coexist as equilibrium states. Their coexistence implies that one of them is metastable. Second, we note that the intra-band SC does not distinguish between different bands, in the sense that the results are equal for both pairings. We note that considering any fixed value of the chemical potential in the region where there is SC, when the anti-symmetric hybridization is increased it eventually destroys the inter-band SC that is present. On the other hand, if we keep increasing the hybridization, it raises the intra-band SC up to a maximum value until it suppresses the SC definitely.

In Fig. 1d we show the spectral gap for the self-consistent results. Also we show the phase diagram in the right plot of the same figure. As we can see, the consideration of inter-band, intra-band superconductivity and anti-symmetric hybridization results in a rich phase diagram. In this figure, the solid lines represent a gap closing, while the dashed lines represent a phase separation without closing the gap. Phase I in this figure is a gapless superconducting phase, driven by the inter-band coupling, and it was shown [49] to behave like Weyl superconductor. The phase II is a two-band superconductor with only intra-band couplings. Phase III is a topological insulator which was shown to have localized states at the edges [49] of a finite chain. The phase IVa shows gapped superconductivity and represents the strong inter-band coupling superconducting phase. The phase IVb is a trivial insulator and there is no SC remaining. Finally, phase V is a normal metallic phase. All those phases are symmetric around $\mu = 0$. Since the intra- and inter-band pairings do not coexist, the phases with no intra-band pairing are similar to the results previously obtained [49]. The main difference results from the appearance of the intra-band pairing in some regions of the phase diagram.

B. Symmetric hybridization

Analogously to the previous case, we also calculate the order parameters self-consistently considering symmetric hybridization ($V_{\rm s}$). This is the case when the orbitals an-

gular momenta have equal parities, like orbitals s and d. In Fig. 2 we show the results for the same set of values g, $g_{\rm A}$ and $g_{\rm B}$ as the anti-symmetric case. First, we notice that the intra-band SC distinguishes between different bands, since there is a change of sign between them. Unlike the anti-symmetric case, here there is a coexistence of inter- and intra-band SC. Remarkably, the inter-band has the larger order parameter for all region of parameters. In general, this indicates that the inter-band SC has higher critical temperature, which turns out to be responsible for the superconductivity appearing in the material. Note that symmetric hybridization is responsible for the emergence of intra-band SC. Very strong symmetric hybridization eventually destroys superconductivity.

In Fig. 2 we also show the spectral gap for the self-consistent results. We also show the phase diagram in the right plot of Fig. 2, as in Fig. 1. As before, the solid lines represent a gap closing, while the dashed lines represent a phase separation without closing the gap. Phase I and IIa are gapped superconducting phases, with the coexistence of inter- and intra-band couplings, but dominated by the inter-band one. Phase IIb is an insulating phase and there is no SC. All those phases are symmetric around $\mu = 0$. The more interesting phase is phase I, which allows both types of couplings and shows nontrivial topological properties. This phase is characterized by localized edge states and finite winding number, as will be shown in the next section.

The robustness of the inter-band superconductivity can be tested varying the relative amplitudes of the g, g_A and g_B parameters. Considering, for instance, the case $g_A = g_B \equiv g_0$ and selecting the point $\mu = 0$ and $V_s = 1$, the appearance of the inter-band SC is not continuous with increasing g, but goes through a first order transition at some point $g > g_0$ near to $g = g_0$ to a value that always has a larger amplitude than the intra-band ones. While the results of Figs. 2 consider a large g value, the results are qualitatively the same, as long as the inter-band SC is present.

III. TOPOLOGICAL PROPERTIES

A. Winding number in the BDI class

The symmetry-protected topological systems are classified accordingly to their symmetries [50]. The Hamiltonian of equation (4) has particle-hole symmetry once it obeys the relation $\mathcal{H}_k = -\mathcal{O}\mathcal{H}_k\mathcal{O}^{-1}$ [50], where the operator written in the Nambu representation [48] is $\mathcal{O} = \mathbf{\Gamma}_{x0}K$, in which $\mathcal{O}^2 = +1$ and K applies the complex conjugate and inverts the momentum. In addition, the Hamiltonian has simplified time reversal symmetry for spinless fermions, $\mathcal{H}_k = \mathcal{H}^*_{-k}$. In the presence of both symmetries, the Hamiltonian belongs to the BDI class of topological systems, and the one-dimensionality guarantees that the space of the quantum ground state is partitioned into topological sectors labeled by an integer ($\mathbb{Z}$) number [50].

In the $\mathbb{Z}$ class of topological systems, the topological phases in odd-dimensional systems (or, in other words, those with chiral symmetry) are characterized by the topological invariant called winding number [50, 51]. This invariant counts the number of the zero-energy states protected by the topological property of the Hamiltonian, and may be calculated in the usual way [51, 52]. One needs to look for an hermitian matrix which anti-commutes with the Hamiltonian ($\mathcal{H}$), i.e., find Γ such that $\{\mathcal{H}, \Gamma\} = 0$. Considering spinless time-reversal symmetry and particle-hole symmetry (PHS) then the Chiral operator that carries both symmetries is Γ_{x0}. It implies that the Hamiltonian anti-commutes with that operator, which can be used to bring the Hamiltonian to an off-diagonal form. Using the basis that diagonalizes Γ_{x0}, i.e., $R^{-1}\ \Gamma_{x0}\ R = D$, with $R = \Gamma_{xx} - \Gamma_{zx}$ and D a diagonal matrix, implies that

$$R^{-1}\ \mathcal{H}_k\ R = \begin{pmatrix} 0 & q\,(k) \\ q^{\dagger}\,(k) & 0 \end{pmatrix}. \tag{11}$$

Writing a generic Hamiltonian in the form

$$\mathcal{H}_k = \sum_{i,j} h_{ij}\mathbf{\Gamma}_{ij}, \qquad i,j = 0,x,y,z, \tag{12}$$

whose coefficients h_{ij} may be extracted from any generic Hamiltonian $\mathcal{H}$ through $h_{ij} = \frac{1}{4}\mathrm{Tr}\,(\mathbf{\Gamma}_{ij}\mathcal{H})$, if we apply the PHS to Eq. (12) as $\mathcal{H}_k = -\Gamma_{x0}\mathcal{H}^T_{-k}\Gamma_{x0}$ and proceed with the block off-diagonal calculations described above we find that

$$q\,(k) = \sum_j c_j\,(h_{zj} + ih_{yj})\,\sigma_j, \qquad j = 0,x,y,z, \tag{13}$$

where $c_0 = c_x = +1$ and $c_y = c_z = -1$, $\sigma_{x,y,z}$ are the Pauli matrices and σ_0 is the 2×2 identity matrix.

The winding number, W, is defined as the number of revolutions of $\det\,[q\,(k)] = m_1\,(k) + im_2\,(k)$ around the origin in the complex plane when k changes from $-\pi$ to π,

$$W = \frac{1}{2\pi}\int_{-\pi}^{\pi} \frac{\partial\theta\,(k)}{\partial k}dk, \tag{14}$$

with

$$\theta\,(k) = \arg\det\,[q\,(k)] = \tan^{-1}\frac{m_2\,(k)}{m_1\,(k)}. \tag{15}$$

For the generic case considered above we have that

$$\begin{aligned} m_1\,(k) &= \sum_j d_j\,(h^2_{zj} - h^2_{yj}) \\ &\text{and} \\ m_2\,(k) &= \sum_j d_j\,(2h_{zj}h_{yj})\,, \end{aligned} \tag{16}$$

where $d_0 = +1$ and $d_{x,y,z} = -1$.

B. Edge states in a finite chain

In order to find the energy spectrum of a finite chain of fermions through the BdG transformation we write the Hamiltonian, Eq. (4) transformed to real space, in the form

$$\mathcal{H} = \boldsymbol{C}^\dagger \boldsymbol{H} \boldsymbol{C}, \tag{17}$$

where

$$\boldsymbol{C} = \begin{pmatrix} a_1 & b_1 & a_1^\dagger & b_1^\dagger & \cdots & a_N & b_N & a_N^\dagger & b_N^\dagger \end{pmatrix}^T \tag{18}$$

and the operators $a_i^\dagger$ (a_i) and $b_i^\dagger$ (b_i) create (annihilate) a fermion in the orbital A and B, respectively, at position i in the chain. The matrix $\boldsymbol{H}$ is defined as

$$\boldsymbol{H} = \begin{pmatrix} \mathcal{H}_{11} & \cdots & \mathcal{H}_{1N} \\ \vdots & \ddots & \vdots \\ \mathcal{H}_{N1} & \cdots & \mathcal{H}_{NN} \end{pmatrix}, \tag{19}$$

and is comprised by the following (4×4) interaction matrices

$$\begin{cases} \mathcal{H}_{r,r} & = -\mu\Gamma_{z0}, \\ \mathcal{H}_{r,r+1} & = -t\Gamma_{zz} - i\frac{\Delta}{2}\Gamma_{yx} - i\frac{\Delta_0}{2}\Gamma_{y0} + V(r+1), \\ \mathcal{H}_{r,r-1} & = -t\Gamma_{zz} + i\frac{\Delta}{2}\Gamma_{yx} + i\frac{\Delta_0}{2}\Gamma_{y0} + V(r-1), \\ \mathcal{H}_{r,r'} & = 0 \qquad \forall\, r' \neq r,\ r+1 \text{ or } r-1, \end{cases} \tag{20}$$

where $V(r+1) = -V(r-1) = -i\frac{V}{2}\Gamma_{zy}$ for anti-symmetric hybridization, and $V(r+1) = V(r-1) = \frac{V}{2}\Gamma_{zx}$ for symmetric one.

If we consider the BdG transformation as the following

$$\begin{aligned} a_r &= \textstyle\sum_n \left[u_{s,n}(r)\gamma_n + v_{s,n}^*(r)\gamma_n^\dagger\right], \\ b_r &= \textstyle\sum_n \left[u_{p,n}(r)\gamma_n + v_{p,n}^*(r)\gamma_n^\dagger\right], \end{aligned} \tag{21}$$

it diagonalizes the Hamiltonian, $\mathcal{H} = E_0 + \sum_n E_n \gamma_n^\dagger \gamma_n$, such that $\boldsymbol{U}^\dagger \boldsymbol{H} \boldsymbol{U} = \boldsymbol{E}$, where $\boldsymbol{U}$ is formed by all the BdG coefficients u_s, v_s, u_p and v_p, and has the property to be unitary $\boldsymbol{U}^\dagger \boldsymbol{U} = \mathbb{I}$. The matrix $\boldsymbol{E}$ is diagonal and contains the energy spectrum (E_n) of the system.

C. 4π Josephson effect

In the previous section we have considered a 1D open chain, i.e., there is no connection between sites 1 and N. In terms of eq. (20) we have $\mathcal{H}_{N,1} = \mathcal{H}_{1,N} = 0$. Now we may think of a chain as a ring with a Josephson junction coupling the ends, see Fig. 3. An extra hopping term t' couples the end point of the ring to the first point via some insulating junction. If a uniform magnetic field (Φ) flows through this ring, its effect may be captured by a Peierls substitution in the extra hopping term, t' [53]. Thus, the Josephson junction may be represented by the following boundary conditions

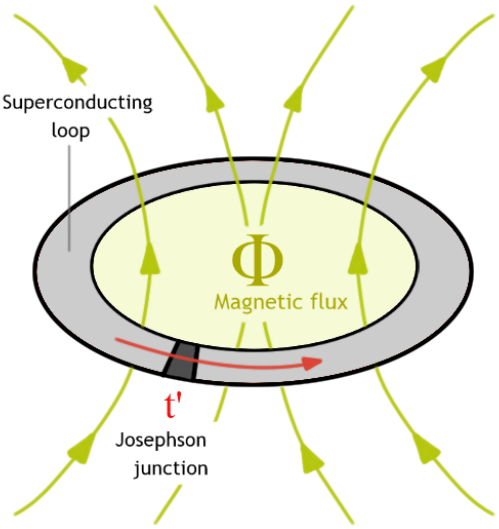

Figure 3. Schematic figure illustrating the 1D superconducting ring with a Josephson junction.

$$\mathcal{H}_{N,1} = \mathcal{H}_{1,N}^* = \begin{pmatrix} -e^{-i\phi/2}t' & 0 & 0 & 0 \\ 0 & e^{-i\phi/2}t' & 0 & 0 \\ 0 & 0 & e^{i\phi/2}t' & 0 \\ 0 & 0 & 0 & -e^{i\phi/2}t' \end{pmatrix}, \tag{22}$$

where the superconducting phase difference ϕ across the junction is related to the magnetic flux through the ring by $\phi = 2\pi\Phi/\Phi_0$, and $\Phi_0 = h/2e$ is the superconducting flux quantum. We have that t' is the tunneling, or inversely proportional to a barrier amplitude, across the junction. As mentioned above this is equivalent to the original proposal of the Josephson junction between two different superconductors with different pairing phases also separated by some tunneling amplitude accross an insulator (or metal).

We may now analyze the junction effect on a current flowing in the ring as we change the magnetic flux by discrete amounts of flux quantum, by changing the junction phase ϕ by multiples of 2π. In a normal superconductor each additional flux quantum ($\Delta\phi = 2\pi$, usually called a pump) should lead the system to its initial state [54]. On the other hand, the topological superconductor (TSC) changes its parity at every pump [55], leading the system to a different final state after pumping. The reason is that the TSC is allowed to have zero energy crossings in its spectrum of excitation during the pump and therefore only returns to its initial state after a further change of the phase by 2π.

D. Symmetric hybridization

a. Winding number: we begin our analysis of the topological phases of the proposed model with the wind-

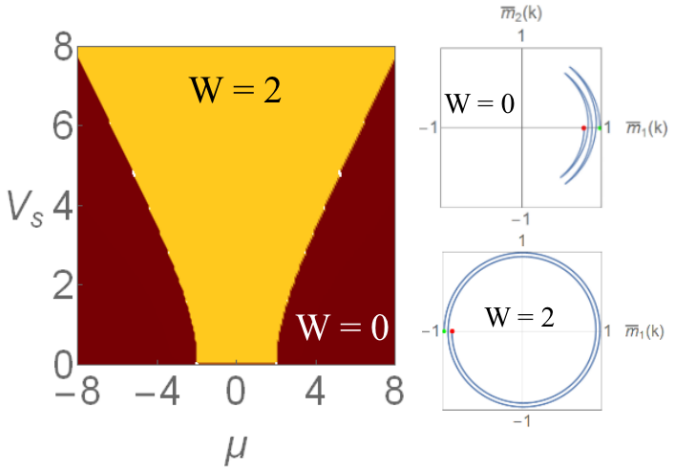

Figure 4. In the left panel we show the winding number calculated from the self-consistent results for symmetric hybridization, over the phase space of parameters. In the right panels we show the normalized parametric plot of real and imaginary parts of $\det[q(k)]$. The number of times $\det[q(k)]$ wraps the origin is the winding number and is illustrated in the right side.

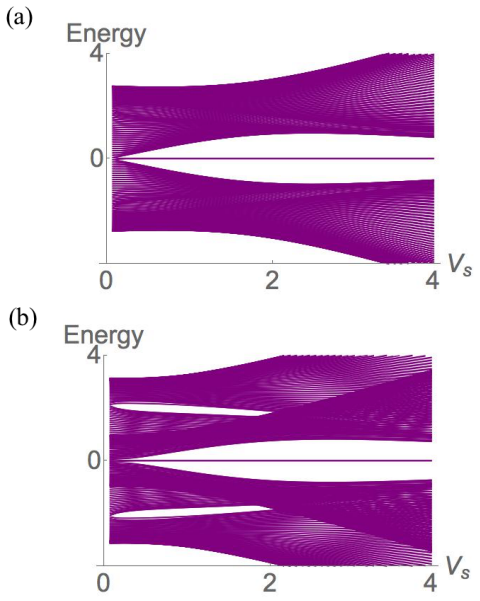

Figure 5. Here we show the energy spectrum of the self-consistent results, for two fixed values of the chemical potential and increasing symmetric hybridization ($\mu = 0$ on (a) and $\mu = -1.4$ on (b)).

ing number calculation. For convenience, we'll consider the case where $\Delta_B = -\Delta_A = \Delta_0$. If we compare Eq. (4) – with symmetric hybridization $V_{s,k}$ – and Eqs. (16) we have $m_1(k) = \mu^2 + \Delta_k^2 + \Delta_{0,k}^2 - V_{s,k}^2 - \epsilon_k^2$ and $m_2(k) = -2(V_{s,k}\Delta_k - \epsilon_k\Delta_{0,k})$. This suggests that the symmetric hybridization may induce a topological phase, since we have non-vanishing m_2 even to zero chemical potential. To be sure that the phase is topological we must calculate the winding number itself, or see if the parametric plot of $\bar{m}_1(k)$ and $\bar{m}_2(k)$ contains the origin when $k \in [-\pi, \pi]$. The results for the winding number and the parametric plot are shown in Fig. 4 for the parameters $V_s = 1.2$, $\mu = -1.04$. This figure shows that the parametric plot wraps the origin twice; it means that the winding number in this case is two, $W = 2$. The results for the winding number clearly show the topological phase, induced by symmetric hybridization, and dominated by inter-band superconductivity for small values of the chemical potential that grows as the hybridization, V_s, grows.

b. Edge states – Since we have defined the topological region of the parameters, we may analyse the zero-energy modes explicitly through the energy spectrum of a finite chain. We have calculated the energy spectrum for a chain of $L = 100$ sites, therefore, we get $4L$ energies for the spectrum. We have checked that this size is large enough to prevent finite size effects. We analyze the energy spectrum for two fixed values of chemical potential, $\mu = 0$ and $\mu = -1.4$, and increasing the hybridization according to the self-consistent solution of Fig. 2. The results are shown in Fig. 5. What we immediately see is that the zero-energy states are robust, i.e., even when μ is non-zero they are present, which characterizes the zero-energy modes in the superconducting phase. We notice that those states are four-fold degenerated. We have checked that they have wavefunctions that are localized exponentially close to the edges if the system is large enough.

c. 4π Josephson effect: we may also analyse the topological properties of the system via Josephson junction scheme, see Fig. 3. First, we look to the excitation spectrum (bogoliubons) during two pumps for each superconducting phase in the phase diagram. The results are shown in the first row of Fig. 6, where 6a is for the trivial phase IIa, whereas 6b and 6c are for the topological phase I for two values of the chemical potential. We may see that there are level crossings when the SC is in its topological phase and there is no crossing in the trivial one.

To explicitly see the periodicity of the Josephson current during the pump, we need to analyse the ground state energy (E_0) of the superconductor preserving its parity, i.e., the ground state is composed by the solid (red) lines of the excitation spectrum. Dashed (blue) lines carry the opposite parity. Thus, the sum over the "negative" excitation to compute E_0 needs to follow the excitation when it crosses the zero energy state. In the topological phase, the crossing through zero energy is a direct consequence of the presence of the zero energy mode at the end of the chain. Here we have two zero energy excitations at each end, thus it is natural that we have two level crossings (we notice that region I with $\mu = 0$ in Fig. 6 has a degenerate level crossing). When $\mu \neq 0$ the level crossing modes do not need to be degenerated, but we notice that even though we have two level

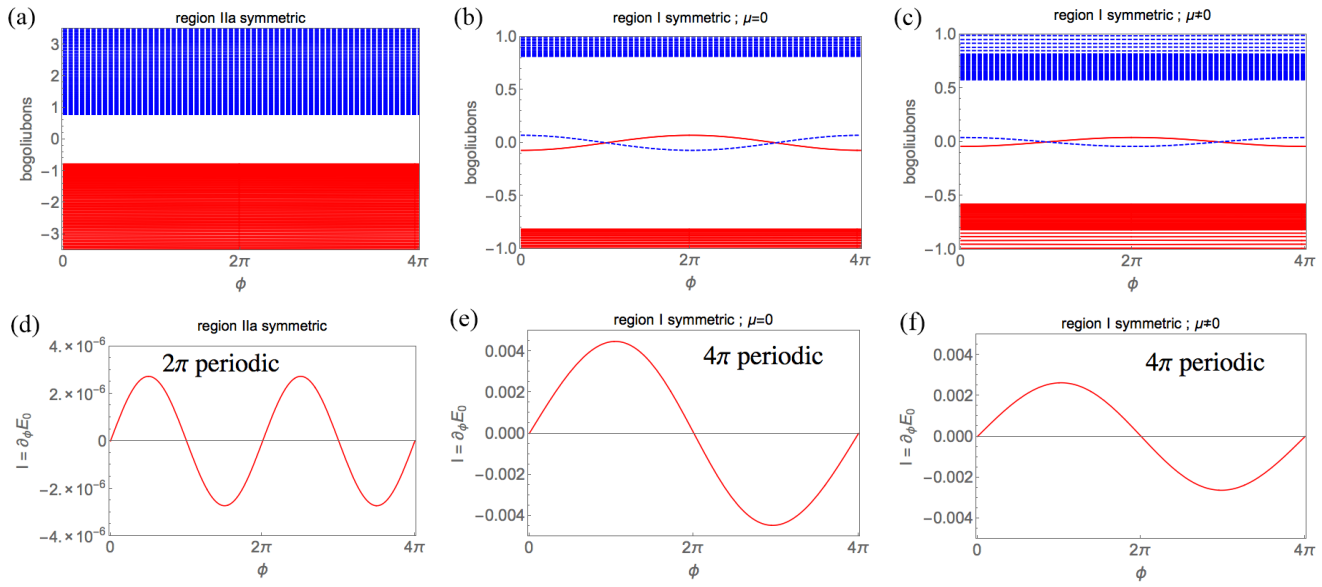

Figure 6. Results for the case of symmetric hybridization case as we vary the tunneling phase ϕ: i) First row shows the excitation spectrum that preserves the parity of the superconductor. ii) Second row shows the Josephson current through the Josephson junction. Here we have used $L = 150$ and $t' = 0.1$.

crossings (and their particle-hole symemtric), the crossings through zero always happen at the same ϕ point. Second row of Fig. 6 shows the current flowing through the junction, which is the derivative of the ground state energy respective to the flux ϕ. We clearly see that the current has a periodicity of 2π (one pump) in the trivial phase, Fig. 6d. On the other hand, the periodicity of the Josephson currents in Figs. 6e and 6f are 4π (two pumps), characterizing the topological superconducting phase and providing an alternative evidence for the presence of Majorana states.

E. Anti-symmetric hybridization

d. Winding number: we proceed the analysis of the topological properties with the winding number calculation. For convenience, and since the self-consistent results do not distinguish the SC in the bands, we'll consider the case where $\Delta_A = \Delta_B = \Delta_0$. Therefore, comparing Eq. (4) – with anti-symmetric hybridization, V_{as} – and Eqs. (16) we have that $m_1(k) = \mu^2 + \Delta_k^2 - \Delta_{0,k}^2 - V_{\mathrm{as},k}^2 - \epsilon_k^2$ and $m_2(k) = -2\mu\Delta_{0,k}$. As a result we notice that only for a non-zero chemical potential and intra-band superconductivity we have non-vanishing m_2 and the system may include a topological phase. Calculating the winding number, as described in Eq. (14), one obtains a trivial solution ($W = 0$) for all self-consistent solutions in parameter space [49]. Even though the winding number seems to indicate a trivial solution, the results of Ref. [49] for a system with no intra-band pairing show that the phases corresponding to regions I and III of the phase diagram in Fig. 1 are topological. The topological

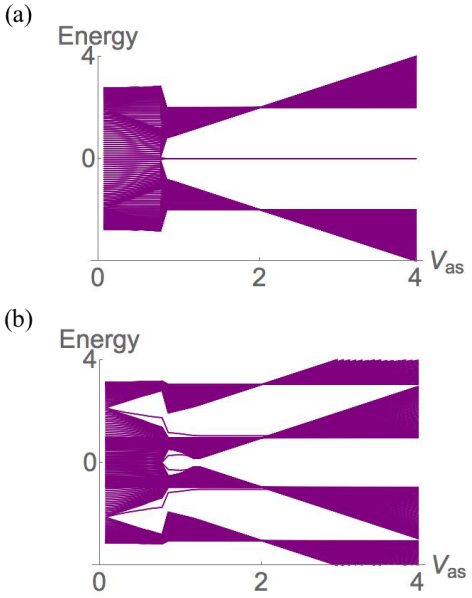

Figure 7. Here we show the energy spectrum of the self-consistent results, for two fixed values of the chemical potential and increasing anti-symmetric hybridization ($\mu = 0$ on (a) and $\mu = -1.4$ on (b)).

property of phase III is hidden by particle-hole symmetry. Moreover, Ref. [49] shows that in this phase localized states are present in the edges of the chain (despite having finite energy when $\mu \neq 0$). As concerns phase I, it is a topological phase that presents Weyl fermions [49] whose topological character remains also undetected by the winding number calculation. In that reference it is

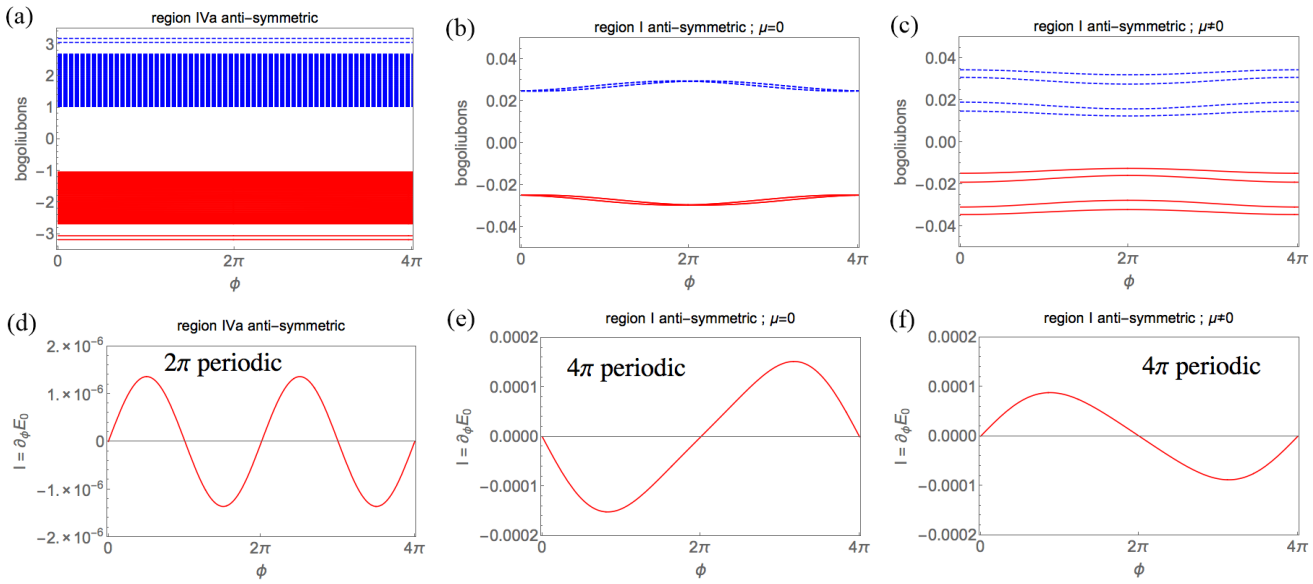

Figure 8. Results for anti-symmetric hybridization as we vary the tunneling phase ϕ: i) First row shows the excitation spectra that preserve the parity of the superconductor. ii) Second row shows the Josephson current flowing through the Josephson junction. Here we have used $L = 250$ and $t' = 0.1$.

shown an alternative procedure to uncover the topological nature of this phase.

e. Edge states – now we proceed with the analysis of the zero-energy modes explicitly through the energy spectrum of a finite chain. We also have used $L = 100$ sites, which is large enough to prevent finite size effects. We analyze the energy spectrum for two fixed values of chemical potential, $\mu = 0$ and $\mu = -1.4$, and increasing the hybridization according to the self-consistent solution of Fig. 1. The results for anti-symmetric hybridization are shown in Fig. 7. We immediately see that the zero-energy states for $\mu = 0$ are not robust, in the sense that they disappear when $\mu \neq 0$. This is the difference of zero-energy modes in the superconductor (phase I for symmetric hybridization) and zero-energy modes in the insulator (phase III for the anti-symmetric hybridization). The chemical potential is not breaking any symmetry, but the zero-energy modes in the superconductor are topologically protected and survive after the introduction of a finite μ, while in the insulator those zero-energy modes are not protected and can be eliminated as you see in this figure.

f. 4π Josephson effect: we may also analyse the topological properties of the system via Josephson junction scheme (Fig. 3). We start looking to the excitation spectrum (bogoliubons) during two pumps for each superconducting phase in the phase diagram. The anti-symmetric case has three types of superconducting phases: intraband gapped SC, interband gapped SC and interband gapless SC, as shown in Fig. 1e. Both gapped superconducting phases (II and IVa) show similar excitation spectra and their typical bogoliubons that keeps the ground state parity are shown in Fig. 8a. As expected, there are no level crossings in the excitation spectrum and the current is 2π periodic as we can see in Fig. 8a for the case of region IVa.

In phase I, even though we have no gap in the bulk spectrum of an infinite system, it is still possible to calculate the Josephson current in a finite one. The junction itself opens up a small gap in the spectrum if L is not too large and t' is not too strong. Of course, in the limit $L \to \infty$ the gap closes, but if the tunneling t' is too large (or the barrier too small) the junction just couples both ends analogously to a periodic boundary condition (i.e., infinite system). Thus, a typical excitation spectrum for very small energies in the gap generated by the coupling accross the junction (positive and negative excitation) is shown in Figs. 8b and 8c.

Even though Figs. 8b and 8c show no level crossings during the pumps, we may proceed with the same calculations as before and obtain the Josephson current. The result is shown in Figs. 8e and 8f for two values of the chemical potential. Clearly, both figures exhibit 4π periodic Josephson current, even without zero energy level crossings revealing in some sense the hidden topological nature of this Weyl-phase.

IV. CONCLUSIONS

In this paper we have studied a model of a p-wave, one dimensional, multiband superconductor. This represents a generalization of the single band model for odd-parity superconductivity that gives rise to a much richer phase diagram with a variety of quantum phase transitions. The odd-parity superconductivity is preserved in this ex-

tension, but inter-band superconductivity is now present in addition to the intra-band ones. The presence of two-bands in our model allows us to include hybridization, increasing the space of parameters. We have considered symmetric and anti-symmetric hybridizations. Both are permitted, depending on the parities we choose for the angular momenta of the two orbitals.

We have calculated the self-consistent solutions for the inter- and intra-band superconducting order parameters as functions of the chemical potential and the strength of the symmetric or anti-symmetric hybridization. The self-consistent calculation of the order parameters allow to obtain the $T = 0$ phase diagram of the system. When increasing anti-symmetric hybridization, both intra- and inter-band superconductivity emerge in the phase diagram, but they compete and exclude one another for different values of band-filling. On the other hand, when increasing the symmetric hybridization, both types of superconductivity are present and they coexist. An interesting result is that inter-band superconductivity has the highest value of order parameter, indicating that it has the higher critical temperature and makes it responsible for the superconductivity appearing in the system.

A general approach for obtaining the winding number of a system described by 4×4 matrices was presented. It may be applied whenever particle-hole symmetry and spinless time-reversal symmetry are present in a Bogoliubov-de Gennes (BdG) Hamiltonian, which is the case of the two-bands BCS superconductors studied here. According to this approach, a dominant inter-band coupling with symmetric hybridization between bands induces a topological superconducting phase. The non-trivial topological character of this phase was shown through a calculation of the winding number, using the self-consistent solutions for the different order parameters. In order to further clarify our results concerning the nature of the topological phases and their end states, we have analyzed the energy spectrum of a finite system. We have compared the energy spectrum between the anti-symmetric and symmetric results, or the trivial and topological results, respectively. We also checked the localization of the zero-energy states.

In order to provide further evidence for the presence of edge Majorana states we have shown that in the topological phases one finds a 4π-periodic (fractional) Josephson current as one changes the magnetic flux accross a ring composed of the superconductor with an insulator inserted between its ends. The result is consistent with the results for the winding number and edge states for the topological phase in the case of symmetric hybridization. In addition, we also found the same 4π-periodic Josephson current in the hidden topological phase identified previously as Weyl-type in the case of anti-symmetric hybridization.

As a final note, we highlight that symmetric hybridization in addition to odd-parity inter-band superconductivity stabilizes a topological non-trivial phase, which presents localized states at the ends of the chain.

ACKNOWLEDGMENTS

The authors would like to thank the CNPq and FAPERJ for financial support. They also are grateful to Emilio Cobanera for discussion and calling attention to Ref. [47], and Griffith M.A.S. for useful discussions. Partial support from FCT through grant UID/CTM/04540/2013 is acknowledged.

REFERENCES

[1] J. Kortus, Physica C: Superconductivity **456**, 54 (2007), recent Advances in MgB2 Research.
[2] X. X. Xi, Reports on Progress in Physics **71**, 116501 (2008).
[3] Y. Yang, W.-S. Wang, Y.-Y. Xiang, Z.-Z. Li, and Q.-H. Wang, Phys. Rev. B **88**, 094519 (2013).
[4] S. Yin, J. E. Baarsma, M. O. J. Heikkinen, J.-P. Martikainen, and P. Törmä, ArXiv:1508.05321 [cond-mat.quant-gas] (2015), arXiv:1508.05321 [cond-mat.quant-gas].
[5] R. Nourafkan, G. Kotliar, and A.-M. S. Tremblay, ArXiv:1508.01789 [cond-mat.supr-con] (2015), arXiv:1508.01789 [cond-mat.supr-con].
[6] T. Watanabe, T. Yoshida, and Y. Yanase, ArXiv:1508.01333 [cond-mat.supr-con] (2015), arXiv:1508.01333 [cond-mat.supr-con].
[7] K. Sun, W. V. Liu, A. Hemmerich, and S. Das Sarma, Nat Phys **8**, 67 (2012).
[8] B. Liu, X. Li, B. Wu, and W. V. Liu, Nat Commun **5** (2014).
[9] Y. Tanaka, Superconductor Science and Technology **28**, 034002 (2015).
[10] V. Stanev, Superconductor Science and Technology **28**, 014006 (2015).
[11] G. Go, J.-H. Park, and J. H. Han, Phys. Rev. B **87**, 155112 (2013).
[12] S.-Y. Lee, J.-H. Park, G. Go, and J. H. Han, ArXiv e-prints (2013), arXiv:1312.6469 [cond-mat.str-el].
[13] Y. He, J. Moore, and C. M. Varma, Phys. Rev. B **85**, 155106 (2012).
[14] A. Y. Kitaev, Physics-Uspekhi **44**, 131 (2001).
[15] A. Kitaev, Annals of Physics **303**, 2 (2003).
[16] J. Alicea, Reports on Progress in Physics **75**, 076501 (2012).
[17] W. P. Su, J. R. Schrieffer, and A. J. Heeger, Phys. Rev. Lett. **42**, 1698 (1979).
[18] R. Wakatsuki, M. Ezawa, Y. Tanaka, and N. Nagaosa, Phys. Rev. B **90**, 014505 (2014).
[19] M. Sato, Y. Takahashi, and S. Fujimoto, Phys. Rev. Lett. **103**, 020401 (2009).

[20] J. D. Sau, R. M. Lutchyn, S. Tewari, and S. Das Sarma, Phys. Rev. Lett. **104**, 040502 (2010).

[21] D. Vollhardt and P. Wolfle, *The superfluid phases of Helium 3* (Courier Corporation, 2013).

[22] A. P. Mackenzie and Y. Maeno, Rev. Mod. Phys. **75**, 657 (2003).

[23] M. Sato and S. Fujimoto, Phys. Rev. B **79**, 094504 (2009).

[24] K. Sun, C.-K. Chiu, H.-H. Hung, and J. Wu, Phys. Rev. B **89**, 104519 (2014).

[25] F. Deus, M. A. Continentino, and H. Caldas, Annals of Physics **362**, 208 (2015).

[26] K. T. Law, P. A. Lee, and T. K. Ng, Phys. Rev. Lett. **103**, 237001 (2009).

[27] M. Wimmer, A. R. Akhmerov, J. P. Dahlhaus, and C. W. J. Beenakker, New Journal of Physics **13**, 053016 (2011).

[28] A. V. Burmistrova, I. A. Devyatov, A. A. Golubov, K. Yada, and Y. Tanaka, Journal of the Physical Society of Japan **82**, 034716 (2013), http://dx.doi.org/10.7566/JPSJ.82.034716.

[29] A. Das, Y. Ronen, Y. Most, Y. Oreg, M. Heiblum, and H. Shtrikman, Nat Phys **8**, 887 (2012).

[30] M. A. N. Araújo and P. D. Sacramento, Phys. Rev. B **79**, 174529 (2009).

[31] A. C. Silva, M. A. N. Araújo, and P. D. Sacramento, EPL (Europhysics Letters) **110**, 37008 (2015).

[32] M. Sato and S. Fujimoto, Journal of the Physical Society of Japan **85**, 072001 (2016), http://dx.doi.org/10.7566/JPSJ.85.072001.

[33] T. Ojanen and T. Kitagawa, Phys. Rev. B **87**, 014512 (2013).

[34] P. D. Sacramento, M. A. N. Araújo, and E. V. Castro, EPL **105**, 37011 (2014).

[35] R. M. Lutchyn, J. D. Sau, and S. Das Sarma, Phys. Rev. Lett. **105**, 077001 (2010).

[36] C. Xu and L. Fu, Phys. Rev. B **81**, 134435 (2010).

[37] L. Jiang, D. Pekker, J. Alicea, G. Refael, Y. Oreg, and F. von Oppen, Phys. Rev. Lett. **107**, 236401 (2011).

[38] Kwon, H.-J., Sengupta, K., and Yakovenko, V. M., Eur. Phys. J. B **37**, 349 (2004).

[39] H.-J. Kwon, V. M. Yakovenko, and K. Sengupta, Low Temperature Physics **30**, 613 (2004).

[40] Y. Oreg, G. Refael, and F. von Oppen, Phys. Rev. Lett. **105**, 177002 (2010).

[41] M. Cheng and R. M. Lutchyn, Phys. Rev. B **86**, 134522 (2012).

[42] F. Domínguez, F. Hassler, and G. Platero, Phys. Rev. B **86**, 140503 (2012).

[43] K. T. Law and P. A. Lee, Phys. Rev. B **84**, 081304 (2011).

[44] M. Gibertini, F. Taddei, M. Polini, and R. Fazio, Phys. Rev. B **85**, 144525 (2012).

[45] C. W. J. Beenakker, D. I. Pikulin, T. Hyart, H. Schomerus, and J. P. Dahlhaus, Phys. Rev. Lett. **110**, 017003 (2013).

[46] E. J. H. Lee, X. Jiang, M. Houzet, R. Aguado, C. M. Lieber, and S. De Franceschi, Nat Nano **9**, 79 (2014).

[47] A. Alase, E. Cobanera, G. Ortiz, and L. Viola, ArXiv e-prints (2016), arXiv:1601.05486 [cond-mat.supr-con].

[48] Y. Nambu, Phys. Rev. **117**, 648 (1960).

[49] T. O. Puel, P. D. Sacramento, and M. A. Continentino, Journal of Physics: Condensed Matter **27**, 422002 (2015).

[50] A. P. Schnyder, S. Ryu, A. Furusaki, and A. W. W. Ludwig, Phys. Rev. B **78**, 195125 (2008).

[51] K. Yada, M. Sato, Y. Tanaka, and T. Yokoyama, Phys. Rev. B **83**, 064505 (2011).

[52] A. Ii, K. Yada, M. Sato, and Y. Tanaka, Phys. Rev. B **83**, 224524 (2011).

[53] K. Jiménez-García, L. J. LeBlanc, R. A. Williams, M. C. Beeler, A. R. Perry, and I. B. Spielman, Phys. Rev. Lett. **108**, 225303 (2012).

[54] N. Byers and C. N. Yang, Phys. Rev. Lett. **7**, 46 (1961).

[55] F. Pientka, A. Romito, M. Duckheim, Y. Oreg, and F. von Oppen, New Journal of Physics **15**, 025001 (2013).